An X-ray BBB Michelson interferometer

John P. Sutter,[a]* Tetsuya Ishikawa,[b] Ulrich Kuetgens,[c] Gerhard Materlik,[d] Yoshinori Nishino,[b] Armen Rostomyan,[e] Kenji Tamasaku[b] and Makina Yabashi[a]

[a]SPring-8/JASRI, 1-1-1 Kouto, Mikazuki-cho, Sayo-gun, Hyogo 679-5198, Japan, [b]SPring-8/RIKEN, 1-1-1 Kouto, Mikazuki-cho, Sayo-gun, Hyogo 679-5148, Japan, [c]Physikalisch-Technische Bundesanstalt, 4.303, Bundesallee 100, D-38116 Braunschweig, Germany, [d]Diamond Light Source Ltd, Rutherford Appleton Laboratory, Chilton, Didcot, Oxfordshire OX11 0QX, UK, and [e]Yerevan State University, 1 Alex Manoogian Street, 375025 Yerevan, Republic of Armenia. E-mail: sutter@spring8.or.jp

A new X-ray Michelson interferometer based on the BBB interferometer of Bonse and Hart and designed for X-rays of wavelength $\sim$1 Å was described in a previous paper. Here, a further test carried out at the SPring-8 1 km beamline BL29XUL is reported. One of the BBB's mirrors was displaced by a piezo to introduce the required path-length difference. The resulting variation of intensity with piezo voltage as measured by an avalanche photodiode could be ascribed to the phase variation resulting from the path-length change, with a small additional contribution from the change of the position of the lattice planes of the front mirror relative to the rest of the crystal. This 'Michelson fringe' interpretation is supported by the observed steady movement across the output beam of the interference fringes produced by a refractive wedge when the piezo voltage was ramped. The front-mirror displacement required for one complete fringe at the given wavelength is only 0.675 Å; therefore, a quiet environment is vital for operating this device, as previous experiments have shown.

Keywords: X-ray Michelson interferometer; free-electron laser.

1. Introduction

The continuing advances in free-electron laser (FEL) projects such as TESLA (Brinkmann *et al.*, 1997; TESLA, 2001) and the LCLS (Pellegrini, 1992) have raised the hope that high-brilliance sources offering high temporal coherence will soon be available for X-rays of wavelengths of the order of 1 Å. In self-amplified spontaneous-emission (SASE) FELs such as the TESLA Test Facility, which has so far demonstrated the SASE effect at photon wavelengths down to 95–105 nm (Ayvazyan *et al.*, 2002), the output electromagnetic wave is initiated by the shot noise in the particle current (Derbenev *et al.*, 1982; Bonifacio *et al.*, 1984; Murphy & Pellegrini, 1985). The random nature of the shot noise makes the phase relationship between different radiation pulses unpredictable, so that the phase coherence of SASE FEL radiation averaged over many pulses is far below the electron pulse length. 'Seeding' the FEL undulator with a pre-existing electromagnetic wave whose wavelength matches the resonance condition of the undulator can remedy this problem (Madey, 1971; Kincaid, 1977), and various authors (Adams, 1997; Adams & Materlik, 1997; Feldhaus *et al.*, 1997; Saldin *et al.*, 2001) have proposed ways of doing this. An X-ray Michelson interferometer has been proposed as a diagnostic tool for testing the effectiveness of such FEL seeding schemes (TESLA, 1995), but only two working designs have appeared in the literature thus far. One, originally designed by Appel & Bonse (1991) and improved by Nusshardt & Bonse (2003), uses an LLL interferometer (Bonse & Hart, 1965*a*,*b*) together with two channel cuts connected by a thin flexible link. The channel cuts are inserted into the gaps of the LLL interferometer and are rotated against each other in order to introduce a path-length difference. The Michelson fringes can be examined in detail with this design, but the use of two separated crystals makes the initial alignment more difficult and the temperature and vibrational stability more critical than they would be for a single-crystal interferometer. The other design, reported by Fezzaa & Lee (2001), uses a single silicon crystal cut into a 440–404 or 880–808 three-beam-case interferometer (Graeff & Bonse, 1977). Here, one pair of mirrors is cut with sloped surfaces; translation perpendicular to the incident beam changes the path-length difference. With this design, path-length differences up to 1 mm are achievable, and alignment is relatively simple, but it is not practical to examine the detailed Michelson fringe pattern over this entire range. Instead, only the more slowly varying visibility is measured. This is sufficient to establish the overall temporal coherence of the radiation, but not to use Fourier transform spectroscopy to measure its full spectrum (Bell, 1972; Chamberlain *et al.*, 1979). Furthermore, the need for two simultaneous Bragg reflections limits the application of this type of Michelson interferometer to discrete energies, at which the bandpass of the interferometer is only a few meV.

Sutter *et al.* (2003) presented a novel design for an X-ray Michelson interferometer that combined the convenient alignment properties of a single crystal with the ability to view the detailed Michelson fringes. This design would also be usable without modification over the whole range of hard X-ray wavelengths from 0.825 to 1.177 Å. It is based on the BBB interferometer of Bonse & Hart (1966) and uses the 220 Bragg reflection of a silicon single crystal, with an asymmetry angle of 7° designed to shorten the path of the energy flow through the splitter and so reduce the amount of absorption. A similar design using a silicon single crystal without any flexure joints was successfully tested by Würges *et al.* (1999). The crystal from which the BBB was cut also included an LLL interferometer (Bonse & Hart, 1965*a*,*b*), which, because it is a well tested and frequently used design, has been used for these preliminary tests of the crystal quality. It has so far been shown that the H interference beam of the LLL interferometer shows clear intensity variations when a 1 mm-thick lucite (Plexiglas) phase shifter is rotated within one of the two internal beam paths of the LLL. Furthermore, the dependence of the H interference beam intensity on the rotation angle of the phase shifter was shown to yield the index of refraction of lucite.

In order to introduce a variable path difference in the BBB, a variable force must be applied to the front mirror of the BBB. This can be done with a piezo applied to the proper point on the front section, which was calculated by Sutter *et al.* (2003) to be 33 mm above the crystal base and halfway between the lateral edges of the front face. The parallelogram arrangement of the flexure joints on the left- and right-hand sides of the crystal permit the BBB front mirror to be displaced by the piezo with minimal tipping, keeping the diffracting net planes of the front mirror parallel to those of the other parts of the BBB. In this report, the change over time of the interference fringes introduced by a lucite refractive wedge into the interference beam of the BBB was measured during rising and falling ramps of the piezo voltage. Two types of measurements were taken. In the first, an avalanche photodiode (APD) was used to measure the intensity of a small part of the interference pattern whose size was determined by the width of a single fringe. In the second, the development of the interference fringes over time was recorded live with a CCD camera over the entire output beam.

  DOI: 10.1107/S0909049504015468

2. Principles

Fig. 1 of Sutter *et al.* (2003) shows a photograph of the BBB interferometer crystal tested for this report. Fig. 2 of that paper shows the beam paths within this BBB, and Fig. 4 of that paper depicts the calculated deformation of the front section of the crystal under the influence of the force applied by the piezo. Fig. 1 of the present paper traces a ray starting from a point S on the source through the two paths of the BBB and into the interference beam onto a detector held perpendicular to the wavevector $\mathbf{k}_H$ of the interference beam. The ray traces compare the path taken by the ray through the back of the BBB with that taken by the ray through the front of the BBB when the front mirror is shifted by a distance Δz perpendicular to its surface. The degree of interference that will be observed on the detector will then be determined by the normalized coherence function $\gamma(\mathbf{r}_P, \mathbf{r}_{P'}, \tau)$, where $\mathbf{r}_P$ and $\mathbf{r}_{P'}$ are the positions of the ray trace endpoints P and P′, respectively, and τ is the difference in the time required for the two ray traces to reach their endpoints. If $\Delta z = 0$, then both $\mathbf{r}_P - \mathbf{r}_{P'}$ and τ will be 0.

We assume, as is usual, that the radiation field is stationary and ergodic (Goodman, 1985). If one assumes that the radiation is cross-spectrally pure (Mandel, 1961), then the function $\gamma(\mathbf{r}_P, \mathbf{r}_{P'}, \tau)$ can be written as the product of a spatial coherence part $\gamma(\mathbf{r}_P, \mathbf{r}_{P'}, 0)$ and a temporal coherence part $\gamma(\tau)$. In addition, if the radiation intensity varies considerably only over many coherence lengths, then the spatial coherence part depends only on the difference $\mathbf{r}_P - \mathbf{r}_{P'}$, and so the position of S on the radiation source is not important.

The difference ΔL between the length L_b of the beam path from S through the back of the BBB up to P and the length L_f of the beam path from S through the front of the BBB up to P′ when the front mirror is displaced by Δz is given to a very close approximation by

$$\begin{aligned}\Delta L &= L_b - L_f \\ &= \Delta z\{\csc(\theta_B - \alpha) + \csc(\theta_B + \alpha) \\ &\quad - \cos(\theta_B + \alpha)[\cot(\theta_B - \alpha) + \cot(\theta_B + \alpha)]\},\end{aligned} \tag{1}$$

where θ_B is the Bragg angle and α is the asymmetry angle. The small refractive corrections to the beam angles, being of the order of μrad, are ignored here. In addition, the BBB is not operated at the center of the Bragg reflection rocking curve, but slightly to the low-angle side. However, this correction also amounts to only a few μrad and may thus also be neglected. The distance between P and P′ is similarly given to a close approximation by

$$\Delta x = \Delta z \sin(\theta_B + \alpha)\big[\cot(\theta_B - \alpha) + \cot(\theta_B + \alpha)\big]. \tag{2}$$

At the BBB optimal operating wavelength of 1 Å, θ_B is 15.1°, $\Delta L = 0.963\Delta z$ and $\Delta x = 3.570\Delta z$.

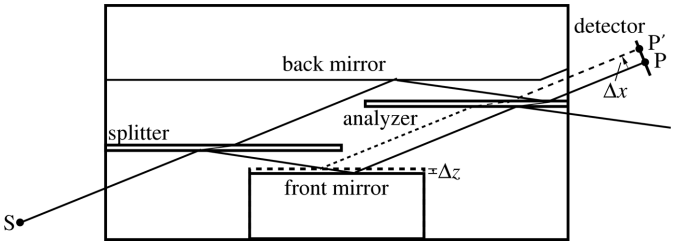

Figure 1
Schematic of the BBB Michelson interferometer showing the shift of the front beam path caused by a displacement Δz of the front mirror. S is the source point; P and P′ are the endpoints of the two paths at the detector. The solid lines shown for the front path are for the case $\Delta z = 0$, for which P and P′ coincide. The dashed lines show the case of non-zero Δz.

Some typical circumstances one would encounter when testing this BBB interferometer on a synchrotron beamline can be used to estimate the maximum value of Δz at which the interference contrast would be lost. First, the temporal coherence of the radiation may be estimated by the formula $\lambda^2/\Delta\lambda$, where $\Delta\lambda$ is the bandwidth of the radiation. With normal double-crystal silicon monochromators at $\lambda \simeq 1$ Å, $\Delta\lambda/\lambda \simeq 10^{-4}$, yielding a temporal coherence length of the order of 1 μm. The value Δz_{tmp}^{max} of Δz at which ΔL exceeds the temporal coherence length is then about 1 μm/0.963 = 1.04 μm; if Δz exceeds this, then interference contrast will disappear. In addition, interference contrast would also be lost if Δx exceeds the spatial coherence length of the radiation, which is of the order of $\lambda r/b$, where r is the distance of the detector from the source as measured along the beam path and b is the source size. On many typical undulator beamlines, r, the distance from the source to the experimental hutch, is around 30 m, while b, the horizontal source size, is of the order of 300 μm. (The horizontal source size is used because the BBB interferometer is oriented so that its diffraction plane will be horizontal.) The estimated spatial coherence length at $\lambda \simeq 1$ Å is then about 10 μm, and the maximum value Δz_{spa}^{max} of Δz at which Δx exceeds this value is 10 μm/3.570 = 2.80 μm. The maximum permissible value of Δz is set by Δz_{tmp}^{max} and Δz_{spa}^{max}, whichever is smaller. It is thus clear that, if this BBB is to be tested on most synchrotron beamlines, the surfaces of the front and back mirrors must be cut during fabrication to a tolerance of a fraction of a micrometer. Improving the temporal coherence of the radiation by using monochromators of narrower bandwidth is of only limited use, because the small spatial coherence continues to limit the fabrication tolerances quite severely.

On a beamline that offers improved spatial coherence, however, this BBB can be tested under much more favorable conditions. One way to improve the spatial coherence is very simply to increase the source-to-interferometer distance. The second experimental hutch at SPring-8's BL29XUL undulator beamline does exactly this, being located at 987 m from the source. With a horizontal source size of 379 μm (Nishino & Tamasaku, 2001), the estimated spatial coherence is 260 μm, which yields Δz_{spa}^{max} = 72.9 μm. Computer-controlled cutting machines can easily match the tolerances required to keep Δz below this value. The temporal coherence of the radiation is not changed by the increased distance from the source, but now there are real benefits to reducing the bandpass $\Delta\lambda/\lambda$ of the beam on the interferometer by using higher-resolution monochromators, as was carried out in this test.

It remains to calculate the displacement of the front mirror that will change the phase of the front path by 2π. For this, a plane-wave model provides a simple approximation. Once again ignoring the small refractive corrections and the small deviation of the incident beam from the center of the Bragg reflection's rocking curve, one finds, by taking both the path length change and the lateral shift of the front beam path into account, that the first contribution to the phase shift is given by $2\pi\Delta L/\lambda$. However, an additional phase shift arises from the fact that, by displacing the front mirror, one puts the diffracting net planes of this part of the crystal out of registry with those of the rest of the crystal. Each Fourier component $\chi_{\mathbf{G}}$ of the front mirror's susceptibility is thus multiplied by a phase factor $\exp(-2\pi i\,\mathbf{G}\cdot\mathbf{u})$, where $\mathbf{u}$ is the displacement of the front mirror. For the given displacement of Δz, $\mathbf{G}\cdot\mathbf{u} = G\Delta z\cos\alpha$. Furthermore, using Bragg's Law for the particular Bragg reflection $\mathbf{G} = 220$, one finds $G = 2\sin\theta_B/\lambda$. The resulting shift in phase of the front beam path caused by the change in phase of the susceptibility is

$$\varphi_f^{sus} = -2\pi[\sin(\theta_B - \alpha) + \sin(\theta_B + \alpha)]\Delta z/\lambda. \tag{3}$$

The difference between the phase φ_b of the unchanged back path and the phase φ_f of the front path is thus

$$\begin{aligned}\Delta\varphi &= \varphi_b - \varphi_f \\ &= 2\pi\{\csc(\theta_B - \alpha) + \csc(\theta_B + \alpha) \\ &\quad - \cos(\theta_B + \alpha)[\cot(\theta_B - \alpha) + \cot(\theta_B + \alpha)] \\ &\quad + \sin(\theta_B - \alpha) + \sin(\theta_B + \alpha)\}\Delta z/\lambda, \end{aligned} \tag{4}$$

and thus, at λ = 1.000 Å, the wavelength at which the test reported here was carried out, the displacement $\Delta z_{2\pi}$ of the front mirror required for one single interference fringe will be 0.675 Å.

3. Apparatus

3.1. Interferometer

The fabrication and geometry of the interferometer used in the experiments described in this paper are explained by Sutter *et al.* (2003). In this first part, the surfaces of the diffracting parts of the LLL had a dull finish, indicating that the strained surface layer left behind after cutting had not entirely been removed by the etching. Therefore, the whole crystal was etched once more in a 1800 ml bath composed of four parts nitric acid, four parts acetic acid and one part hydrofluoric acid, after which the crystal surfaces were all shiny. The inner reflecting surfaces of the interferometer were then recut at the Physikalisch-Technische Bundesanstalt to make the gap widths for both paths match more closely. Then the crystal was etched again as before. Only after this were the results described in this paper recorded. Note that the final recutting and etching did not alter the essential geometric plan of the BBB, but only the precise component thicknesses and gap widths. The gap between the front mirror and the splitter, measured normal to these components' surfaces, is 3.9 mm, as is the gap between the back mirror and the analyzer. The gap between the front mirror and the analyzer, measured normal to these components' surfaces, is 11.5 mm, as is the gap between the back mirror and the splitter. The precision with which these gaps were cut is estimated through past experience with the cutting and etching of test pieces to be about 2 µm, substantially less than the 21.1 µm estimated temporal coherence length of the radiation used in this experiment.

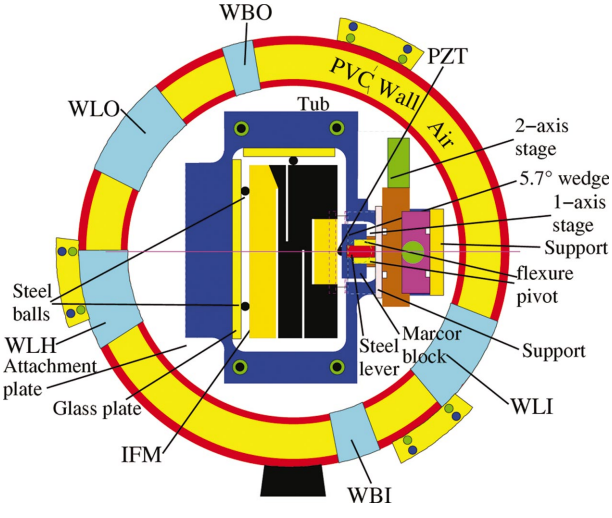

Figure 2
Top view of the interferometer set-up. IFM = interferometer; WLI = window for the incident beam on the LLL; WLO and WLH = windows for the O and H beams, respectively, from the LLL; WBI = window for the incident beam on the BBB; WBO = window for the O interference beam from the BBB; PZT = piezoelectric disc translator with epoxied Marcor hemisphere. The one-axis stage and the wedge attached to it are not visible in this figure, although their positions are indicated.

3.2. Insulation and piezo control

The mounting apparatus of the interferometer crystal is shown in Figs. 2 and 3. It differs from that used by Sutter *et al.* (2003) in the following ways:

(i) Two steel balls attached to the interferometer in the previous paper were removed. Those left allow the crystal to be firmly and reproducibly mounted in the tub without strain. Because the regions where the epoxy was applied are small and far from the diffracting components of the interferometer, the strain transmitted from the epoxy to the BBB is not expected to be large enough to disturb the interference patterns significantly. Notice that the back balls are some 6 mm above the optimal contact point of the piezo, so that the crystal will not tip when force is applied to the front section.

(ii) The compression springs were removed from the crystal, partly to remove the strain caused by the spring forces, and partly to make room for the piezo set-up.

(iii) The piezo set-up was installed. It may best be viewed at the right-hand side of Fig. 3.

(iv) A lucite wedge was inserted into the back beam path of the BBB behind the splitter. The thickness gradient of the wedge lay in the horizontal plane. For the APD scans of the small beam, a wedge with an apex angle of 2.6° was placed with its length roughly perpendicular to the beam direction.

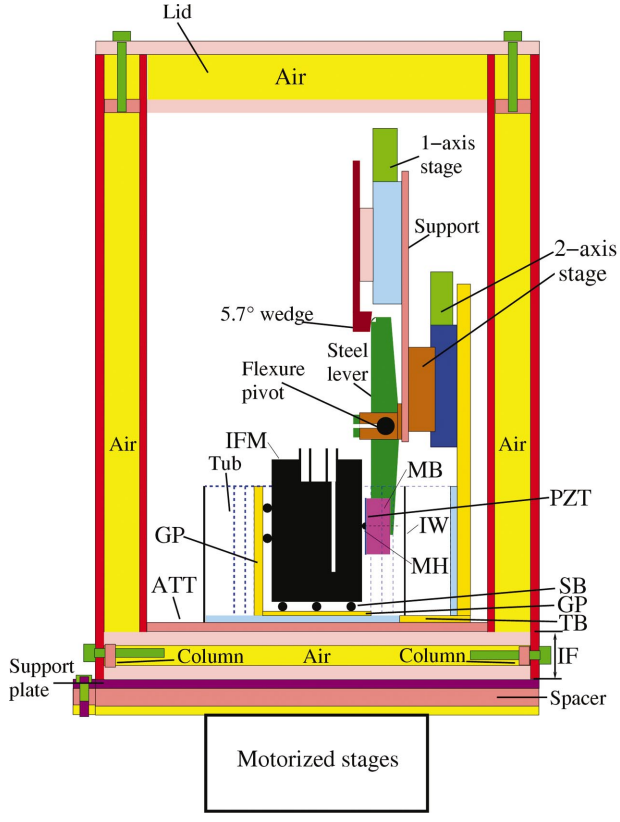

Figure 3
Side view of the interferometer set-up. ATT = attachment plate; GP = glass plates; IW = inner wall of tub; SB = steel balls; TB = base of tub; IF = insulating floor; IFM = interferometer; MB = Marcor block; PZT = piezoelectric disc translator; MH = Marcor hemisphere epoxied to PZT.

The piezo is a disc translator (model CBM 100/25/030M) from Dr Lutz Pickelmann GmbH (2002). Piezoelectric translators have the advantage of being small and light, and of producing no heat which could create unwelcome temperature gradients in the crystal. They also do not introduce any contaminants like oil into the apparatus. A Marcor hemisphere is epoxied to the center to provide a point contact which touches the front section of the interferometer. This type of piezoelectric element was chosen because it offers large displacements (30 μm if the piezo can deform freely) and can exert sufficiently large forces (up to 3 N).

We wished to be able to control the contact point of the piezo on the crystal and also to bring the piezo into and out of contact with the crystal as needed, while disturbing the interferometer as little as possible. For this, the set-up on the right-hand side of Fig. 3 was built. The two-axis positioning stage allows the contact point of the piezo to be varied over a range of 5 mm both vertically and horizontally around the optimal contact point determined by the FEM calculations. Both parts of the stage are driven manually by micrometer screws. This requires the user to remove the lid to adjust the stages; however, the stages have no motors that generate unwanted heat, and they also occupy less space than motorized stages. A vertical stainless steel support plate is mounted on this two-axis stage, and the remaining elements of the piezo set-up are mounted on this. At the bottom of the plate, a flexure pivot is attached. Both ends of the pivot are clamped in place, while a steel lever is clamped to the middle of the pivot. This lever can thus be rotated against the fixed ends of the pivot through several degrees. Because the disc translator described above is attached to the lower end of the lever (see Fig. 3), it can be swung into and out of contact with the front of the crystal as needed. A stainless steel wedge is brought into contact with the rounded upper corner of the lever and can be raised or lowered by a simple micrometer-driven stage with a 5 mm range. As the height of the wedge is changed, the lever is rotated around the ends of the flexure pivot. A wedge angle of 5.7° was chosen so that a 1 mm change in the wedge height corresponds approximately to a 0.1 mm motion of the disc translator, so that the translator has a range of almost 0.5 mm. The position of the disc translator can be roughly adjusted by using spacers of different thickness between the wedge and the stage.

It is, of course, clear that the piezo set-up must be stiff enough to ensure that it is the movable front section of the crystal, not the steel lever or the attachment plates, that yields when voltage is applied to the disc translator. To check this, we used an inductive path sensor. This micrometer-sensitive device uses inductive coils attached to a feeler that can be bent up to 90° to allow easy access into crevices. Checks at several points on the rear support for the two-axis positioning table, the support for the single-axis positioning table, and the steel wedge showed displacements of no more than 0.6 μm when the voltage on the disc translator was ramped from 0 to 200 V. A check on the back wall of the groove behind the movable mirror showed a displacement of under 0.2 μm. A motion of 1.6 μm away from the crystal was detected at the back of the steel lever just below the flexure pivot, at the same height as the top of the tub. Though considerable, this still permitted the disc translator to push the crystal's movable mirror; a measurement on the middle of the front face of this mirror showed a displacement of 1 μm towards the back of the crystal. The disc translator is thus shown to be effective.

A diagram of the electronics used to apply voltage to the disc translator is shown in Fig. 4. The computer contains a 16-bit digital-to-analog converter (DAC) card with range 0–10 V. The analog signal is amplified and smoothed by an RC element (R = 470 kΩ, C = 300 nF).

3.3. Sources and environment

The tests of this paper were performed at the SPring-8 RIKEN coherent X-ray optics beamline BL29XUL (Tamasaku *et al.*, 2001). This is a standard undulator beamline with two experimental hutches, one (EH1) 52 m from the electron beam source and the other (EH2) 987 m from the source. The in-vacuum undulator of this beamline has a 32 mm period and contains 140 periods (Tanaka, 2001). The electron beam size is 379 μm in the horizontal and 10.1 μm in the vertical; its divergence is 15.5 μrad in the horizontal and 1.75 μrad in the vertical (Nishino & Tamasaku, 2001). Because the BBB is mounted so that it diffracts in the horizontal plane, it is the horizontal beam size and divergence that are most important here. In front of EH1, a non-dispersive double-crystal symmetric Si 111 monochromator reflecting vertically in the Bragg case passes a bandwidth of several eV. The monochromator was adjusted to pass a photon energy of 12.398 keV (λ = 1.000 Å) while the undulator gap was set to 17.4 mm. The photon beam is almost entirely polarized in the horizontal plane, and is therefore π-polarized with respect to the BBB.

The farther hutch EH2 (Ishikawa *et al.*, 2001) was chosen for these tests for four reasons. First, its greater distance from the source improves the spatial coherence of the photon beam, a feature whose advantages have been discussed in §2. Second, because EH2 is in a separate building detached from the other experimental hutches, being connected to the storage ring only by the photon beam vacuum transport pipe, the level of mechanical and electrical noise is much lower than in the other beamlines. Furthermore, it was possible to shut off the air conditioning system inside the EH2 building, a measure found necessary to make the BBB sufficiently stable to observe useful interference patterns. Finally, the photon beam size, which is still quite small in EH1 (1.3 mm horizontal × 0.72 mm vertical), increases to 30 mm horizontal × 10 mm vertical in EH2 because of the finite divergence. Although this reduces the photon beam brilliance, the expansion of the beam allows a wider area of the BBB working area to be covered so that poor-contrast and high-contrast parts of the BBB can readily be distinguished. In addition to these advantages, the experimental hutch inside the EH2 building lies on a separate concrete block from the experimenters' work area, the joint between the two blocks being filled with caulking. Disturbances caused by the users' activities are thus reduced.

The experimental set-up inside the EH2 hutch is shown in Fig. 5. Two separate tables were used for the equipment. An initial slit, a horizontal symmetric Si 333 channel cut, and the BBB itself, contained within the set-up displayed in Figs. 2 and 3, were mounted on the front table. The initial slit passed a 2 mm × 2 mm section of the photon beam entering the hutch. The channel cut was used to further monochromatize the beam to the BBB and so improve the temporal coherence, as discussed in §2. Since, for Si crystals

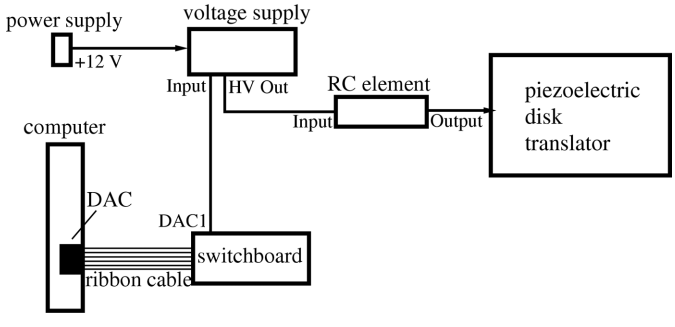

Figure 4
Schematic diagram of the piezo control electronics.

at 295.5 K, the energy width of the symmetric 111 reflection for σ-polarization is 1.7 eV while that of the symmetric 333 reflection for π-polarization is 0.059 eV, we estimate that this increased the temporal coherence by a factor of 30 to 21.1 μm. This channel cut was arranged non-dispersively with respect to the BBB to improve the throughput, although the low divergence (several μrad) makes this issue relatively unimportant. The two detectors were mounted on the back table so that the mechanical noise they produced would disturb the interferometer less. The motorized slit at the front of this table allowed a specific portion of the BBB's interference beam to be selected for either detector. A CCD camera at the front of this table photographed the full BBB interference beam with a pixel size of 12 μm. A fanless model using Peltier cooling was used for its lower noise. The avalanche photodiode (APD) at the back of this table was used to measure the intensity of a small part of the BBB interference beam selected by the motorized slit. When required, the CCD camera could be moved by a stepping-motor stage out of the beam to give the APD an unobstructed view.

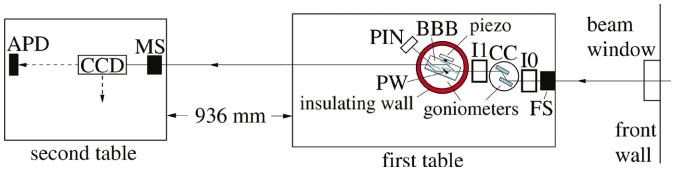

Figure 5
Top view of the experimental set-up at the SPring-8 BL29XUL beamline, hutch EH2. Abbreviations not in the text are as follows: FS = front 2 mm × 2 mm slit; I0 and I1 = ionization chambers; CC = Si 333 symmetric channel cut; PIN = PIN diode used to monitor the 220 Bragg reflection of the BBB; PW = lucite (Plexiglas) wedge; MS = motorized slit. If the CCD camera is moved out, the dashed line to its left shows the beam path to the APD. The BBB assembly shown in Figs. 2 and 3 is here shown only schematically for simplicity.

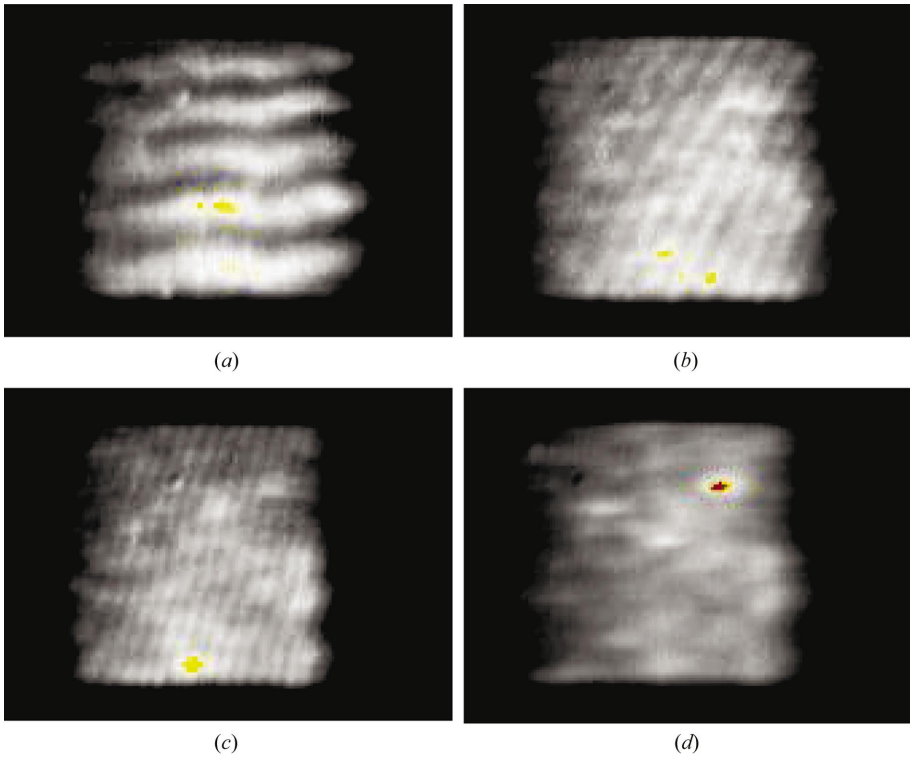

Figure 6
CCD pictures of interference fringe patterns of the BBB with (*a*) no lucite wedge, (*b*) a 2.6° lucite wedge inserted behind the splitter, with its thickness gradient in the horizontal plane, (*c*) a 5° lucite wedge inserted in the same way as the wedge in (*b*), and (*d*) the same wedge as in (*b*) but with a lead foil placed over the back mirror. The integration times for (*a*)–(*c*) were 31 s; that for (*d*) was 21 s. The full 2 mm × 2 mm beam interference pattern is shown here.

4. Results

4.1. Interference pattern check

Before attempting to test whether the piezo allowed us to view Michelson interference fringes, we first checked whether the BBB interference beam would show the expected fringe patterns if a lucite wedge were placed in one of the beam paths as in Fig. 5. Fig. 6 shows the results when the disc translator was out of contact with the front surface of the BBB. As the lucite wedge was simply placed by hand on the base of the gap, an accurate comparison of the fringe widths with theoretical calculations based on the index of refraction and the thickness gradient of the lucite wedge is not possible, since the exact angle of the wedge with respect to the beam was not well known. Even so, several facts can be established. First, the empty interferometer (with no wedge inserted) does not show a pattern of uniform intensity as would be expected if the BBB had been perfectly made, but instead yields the pattern of horizontal stripes shown in Fig. 6(*a*), which would have to be accounted for in real measurements performed with this device. Such non-uniform patterns, commonly produced by X-ray interferometers of all types, reveal the fabrication errors, which in this case were not sufficient to destroy the fringe contrast altogether. The introduction of either lucite wedge behind the splitter produces a pattern of almost vertical stripes as is consistent with the horizontal thickness gradient of the wedge. As one would expect, Fig. 6(*c*), taken with a thicker wedge, shows narrower fringes than Fig. 6(*b*). That the patterns shown by Figs. 6(*a*)–6(*c*) are indeed due to the interference of the two beam paths in the BBB is confirmed by Fig. 6(*d*), in which a lead foil placed over the back mirror blocked the back beam path. The resulting picture thus shows only the contribution from the front beam path, which as expected shows no fringes. One final interesting point is given by the integration times for Figs. 6(*a*)–6(*c*). At 31 s, these times are quite long, and the clarity of the interference fringe images indicates that the fringe positions and intensities remained stable throughout each exposure. This fact testifies to the quiet environment at the BL29XUL EH2 hutch, a thing that, as will be discussed later, is not easily achieved.

4.2. Michelson fringe scans

Having observed that the BBB interferometer does indeed produce visible and stable interference fringes, we reduced the size of the motorized slit to select a part of a single bright fringe in the pattern produced by the 2.6° lucite wedge in Fig. 6(*b*). The motorized slit size was approximately 0.2 mm × 0.2 mm. The piezoelectric disc translator was then brought into contact with the front surface of the interferometer as described in §3.2. Then, with the equipment shown in Fig. 4, the DAC card was set

to increase or decrease the input to the disc translator's voltage supply within the range 0–10 V at a constant rate of 0.0028 V s^{-1}, so that the entire ramp up or down took 1 h. Because the voltage supply amplifies the input voltage by a factor of ten, the voltage thus supplied to the disc translator was ramped between 2.674 V and 100.7 V.

Previous inductive coil sensor measurements of the BBB's front mirror displacement as a function of time during upward and downward ramps of the piezo voltage had shown that the response of the disc translator to voltage changes is neither linear nor instantaneous. Instead, the disc translator would begin to deform only several minutes after the start of a voltage ramp, and would continue to deform many minutes after the voltage had reached its final value. A series of upward and downward ramps also showed that the disc translator has considerable hysteresis, generally several tenths of a micrometer. As a result, without a monitor such as an optical Michelson interferometer using the BBB's front surface as one of the mirrors, there is no clear way to determine how much the disc translator has displaced the front surface at a given time. Optical interferometers have been used for this purpose in conjunction with X-ray scanning interferometers (Deslattes, 1969) to measure the silicon lattice spacing, but this has not been performed with X-ray Michelson interferometers so far. This section therefore seeks to establish only that Michelson fringes can be observed with this set-up; proper Fourier transform spectroscopy (Bell, 1972; Chamberlain *et al.*, 1979) must await further refinements.

Fig. 7 shows the results of the first scan, which was started at the same time as the piezo voltage ramp-up. The APD counts were normalized by I1, the ionization chamber behind the Si 333 channel cut, in order to compensate for ring-current changes, as shown in Fig. 7(*b*). Because of the long lag in the response of the disc translator, data collection was continued long after the voltage ramp had ended, with the voltage remaining at its maximum value. Through most of the scan, no clear fringes were visible; we observed the noiselike variation seen in Fig. 7(*c*). However, 7740 s after the start of the scan, periodic oscillations with a contrast level of 5–6% appeared and persisted until the scan was stopped. An example of these oscillations is shown in Fig. 7(*d*). 52 such oscillations were counted in this scan. The fact that both the periodic oscillations and the noiselike fluctuations have similar amplitudes suggests the possibility that the latter may appear random only because the front mirror was moving too fast to allow individual oscillations to be resolved. It is for this reason that we call the fluctuations 'noiselike' and not simply noise.

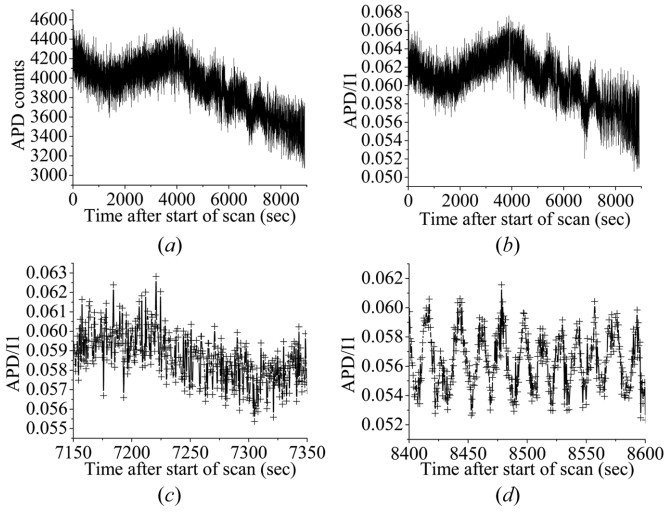

Figure 7
Data scan of APD intensity *versus* time. The motorized slit between the BBB and the APD was set to select a single bright fringe in the interference pattern of the 2.6° lucite wedge. The selected region was about 0.2 mm × 0.2 mm. The voltage supplied to the piezo was ramped up at a constant rate over its full range in 1 h, starting at the beginning of the scan. Each data point was taken over an integration time of 0.4 s. The results are as follows: (*a*) the APD count rate, (*b*) the APD count rate normalized to I1, (*c*) a noiselike region of (*b*), (*d*) a region of (*b*) that shows periodic fringes. The periodic fringes were visible in this scan from 7740 s up to the end.

Similar transitions between periodic oscillations and noiselike fluctuations appeared in both of the next two APD scans. Fig. 8 shows the record of APD intensity over time with the piezo voltage held constant at the maximum value. This scan was started 12 min after the end of the first scan. Up to 4520 s, 634 periodic fringes were counted; an example of these is shown in Fig. 8(*b*). After this, the fringes dissolved into the noiselike pattern shown in Fig. 7(*c*). After this scan was stopped, the CCD camera was moved back into the interference beam exiting the BBB, and the motorized slit was opened to let the full beam through. This confirmed that the interference pattern of the lucite wedge was indeed no longer visible. The CCD was then taken out of the beam, the motorized slit was again reduced, and a new scan was started at the same time as the piezo voltage ramp-down was started. The results of this scan are shown in Fig. 9. After an initial noiselike region, the periodic oscillations reappear at 1785 s and continue up to 3810 s, again returning to noiselike fluctuations after that. 839 periodic oscillations were counted in this last scan.

When the back path of the BBB was blocked with lead foil, leaving only the front path open, similar scans were performed during one

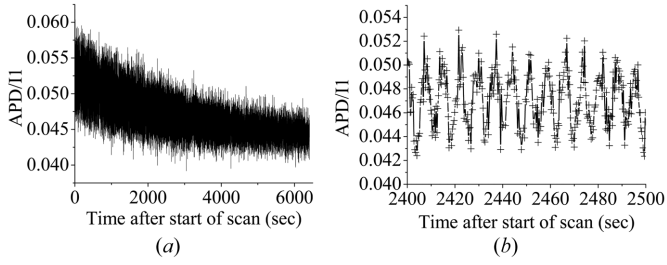

Figure 8
APD scan performed as in Fig. 7, but with an integration time of 0.2 s for each data point and the piezo voltage held constant at the maximum value. This scan was started 12 min after the end of the scan in Fig. 7. (*a*) Entire normalized scan; (*b*) a region of this scan that shows periodic fringes. These fringes were visible in this scan from the beginning up to 4520 s, fading into a noiselike pattern soon after.

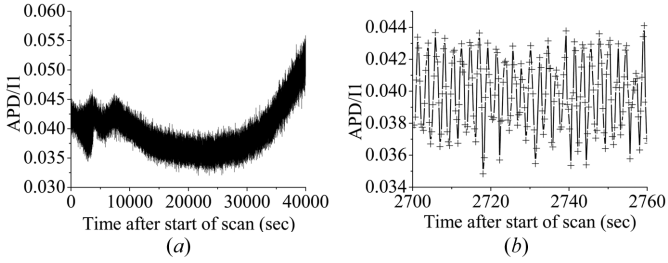

Figure 9
APD scan performed as in Fig. 7 but with an integration time of 0.2 s for each data point, and with the piezo voltage ramped down to its minimum value over a 1 h period starting at the beginning of this scan. 20 min elapsed between the end of the scan in Fig. 8 and the beginning of this one. (*a*) Entire normalized scan, (*b*) a region of this scan that shows periodic fringes, which were visible from 1785 to 3810 s.

upward and one downward ramp of the piezo voltage. Neither scan showed any periodic oscillations of the kind seen in Figs. 7–9. This is one indication that the periodic oscillations are an interference effect. A further piece of evidence indicating that the periodic oscillations are in fact Michelson fringes, arising from the displacement of the front mirror of the BBB, is given in Fig. 10. This sequence of consecutive CCD pictures of the full interference beam from the BBB illustrates the steady unidirectional motion of the interference fringes of the lucite wedge when the piezo is in contact with the front surface of the BBB. A similar fringe motion was observed between the first scan shown in Fig. 7 and the second scan shown in Fig. 8. Because periodic oscillations in the APD intensity were observed at the end of the first scan and once again at the beginning of the second, we believe that the periodic oscillations and the fringe motion are related. Furthermore, no similar regular motion of the interference fringes was ever observed whenever the piezo was not in contact with the front surface of the BBB, as evidenced by the data of §4.1.

5. Conclusions

The data presented here indicate that Michelson fringes of X-rays of wavelength $\sim$1 Å can be observed with a BBB interferometer whose front mirror is connected to the rest of the crystal only by a set of weak links and which is displaced by a piezoelectric disc translator. If the displacement of the front mirror can be accurately measured, and if the motion of the disc translator can be better controlled, convenient measurements of Michelson fringe patterns that would make X-ray Fourier transform spectroscopy feasible should become possible.

A few warnings about the stringent requirements for operating this BBB should be given. Before we brought it to SPring-8 for the tests reported here, we made several attempts to test it at HASYLAB's bending-magnet beamline E2 (RÖMO) and undulator beamline BW1. None of these yielded any interference fringes from the BBB. It appears that the main cause of this failure was the high level of noise coming from the vacuum pumps and electrical devices of both the beamline we were using and the beamlines nearby. That Sutter *et al.* (2003) measured good interference contrast from the LLL attached to this BBB, but never from the BBB itself, in tests performed at HASYLAB may be explained by the greater sensitivity of the BBB to mechanical vibrations. Although a displacement of the front mirror of the BBB also moves the test LLL's splitter, calculations have shown that a displacement of 6.8 Å is required to cause one full LLL fringe shift when X-rays of wavelength 1 Å are used. This is an order of magnitude greater than the displacement required for one full BBB fringe shift. Note that the LLL fringe shift arises from the motion of the standing-wave pattern at the surface of the analyzer when the splitter is displaced. The LLL then behaves like a scanning interferometer (Hart, 1968; Deslattes, 1969). Tests performed using the $K\alpha$ line of a Mo X-ray tube (wavelength 0.709 Å) at the Physikalisch-Technische Bundesanstalt by two of us, Sutter and Kuetgens, confirmed that these LLL standing-wave fringes actually do appear when the disc translator is operated as described in this paper.

Even at SPring-8's 1 km beamline hutch, however, troublesome mechanical noise could appear even with the air-conditioning system turned off, as in the tests reported here. Wind posed the greatest problem; if it blew from a certain direction it would set up a distinctive sound in the ventilation shafts. Whenever we heard this at the same time as the CCD camera was recording the full BBB interference beam, the interference pattern would blur. The pattern would then reappear, with the fringes in the same place as before, when the sound died away. Most of the time this problem was not too serious, but it was made very apparent to us in our first BBB tests at SPring-8, when a typhoon forced a two-day halt to data collection.

In Sutter *et al.* (2003), the tub shown in Figs. 2 and 3 of this paper was filled with silicone oil in order to damp any vibrations of the front mirror that might be induced by the surrounding noise. However, the use of silicone oil was avoided in the tests of the BBB reported here because experience has demonstrated that the oil creeps along the surface of the silicon crystal, forming films over the diffracting parts that destroy the interference patterns. Moreover, the quiet environment of the SPring-8 BL29XUL beamline makes the use of such a damping fluid less necessary.

In summary, although several problems remain to be solved before the BBB interferometer of this paper can be reliably applied to X-ray Michelson Fourier transform spectroscopy, the results of this paper give reason for optimism.

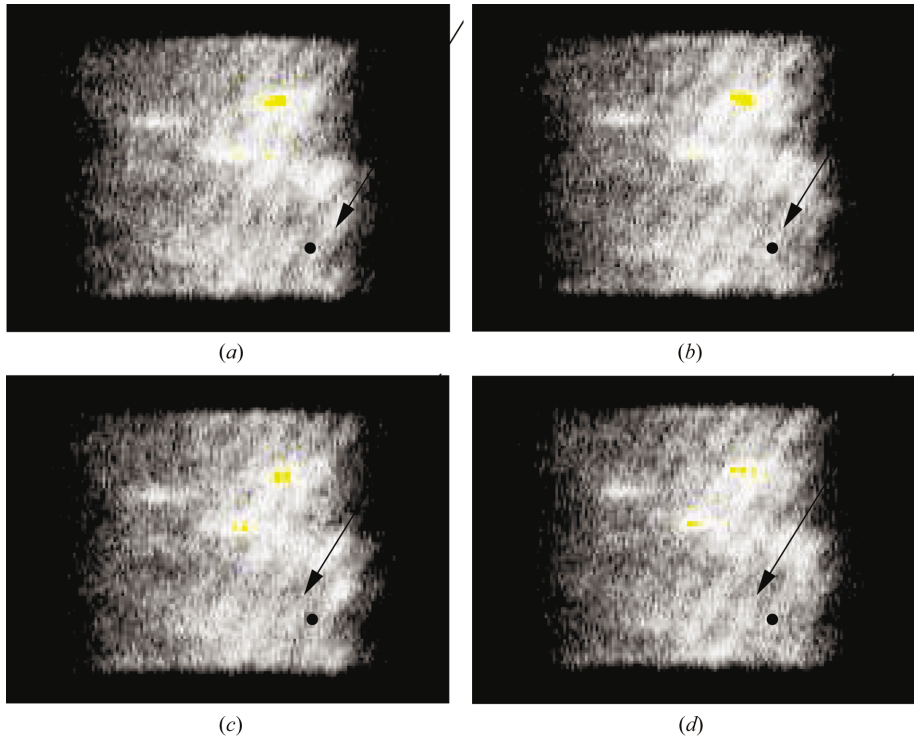

Figure 10
Sequence of CCD pictures showing the motion of the interference fringes of the 2.6° lucite wedge. The integration time for each picture was 1454 ms. The sequence was taken approximately 110 min after the beginning of a 1 h upward ramp of the piezo voltage; after the upward ramp ended, the voltage was maintained at its maximum value. The black dot represents the same fixed point within the beam in all four pictures. The arrow points to one of the bright fringes. Note the movement of this bright fringe from right to left relative to the black dot.

The authors thank Hans-Georg Schmidt of HASYLAB for providing many useful proposals for building the support for the disc translator. Jens Brehling and his staff at the HASYLAB workshop, and the staff at the workshop of DESY's former II. Institut für Physik, built the pieces needed. Albert Dettmer of the Physikalisch-Technische Bundesanstalt recut the BBB to reduce its geometric errors prior to these tests; Fred Knof of DESY measured the gap widths of the BBB. The experiments reported in this paper were performed at SPring-8 with the approval of RIKEN (Proposal No. 2003A0064-NMD3-np and subsequent internal RIKEN proposal).

References

Adams, B. (1997). *Proceedings of the XVIII International Free Electron Laser Conference*, Rome, 1996, pp. II-26–II-27. Amsterdam: North-Holland.
Adams, B. & Materlik, G. (1997). *Proceedings of the XVIII International Free Electron Laser Conference*, Rome, 1996, pp. II-24–II-25. Amsterdam: North-Holland.
Appel, A. & Bonse, U. (1991). *Phys. Rev. Lett.* **67**, 1673–1676.
Ayvazyan, V. *et al.* (2002). *Phys. Rev. Lett.* **88**, 104802.
Bell, R. J. (1972). *Introductory Fourier Transform Spectroscopy.* New York: Academic Press.
Bonifacio, R., Pellegrini, C. & Narducci, L. M. (1984). *Opt. Commun.* **50**, 373–378.
Bonse, U. & Hart, M. (1965*a*). *Appl. Phys. Lett.* **6**, 155–156; **7**, 99–100.
Bonse, U. & Hart, M. (1965*b*). *Z. Phys.* **188**, 154–164.
Bonse, U. & Hart, M. (1966). *Z. Phys.* **194**, 1–17.
Brinkmann, R., Materlik, G., Rossbach, J., Schneider, J. R. & Wiik, B.-H. (1997). *Nucl. Instrum. Methods Phys. Res. A*, **393**, 86–92.
Chamberlain, J. E., Chantry, G. W. & Stone, N. W. B. (1979). *The Principles of Interferometric Spectroscopy.* New York: John Wiley and Sons.
Derbenev, Ya. S., Kondratenko, A. M. & Saldin, E. L. (1982). *Nucl. Instrum. Methods Phys. Res.* **193**, 415–421.
Deslattes, R. D. (1969). *Appl. Phys. Lett.* **15**, 386–388.
Dr Lutz Pickelmann GmbH (2002). *Piezoelectric Bending Actuators, Disk Translators, Piezoelectric Tubes.* Catalogue. Berg-Am-Laim-Strasse 64, D-81673 Munich, Germany.
Feldhaus, J., Saldin, E. L., Schneider, J. R., Schneidmiller, E. A. & Yurkov, M. V. (1997). *Opt. Commun.* **140**, 341–352.
Fezzaa, K. & Lee, W.-K. (2001). *J. Appl. Cryst.* **34**, 166–171.
Goodman, J. W. (1985). *Statistical Optics.* New York: John Wiley and Sons.
Graeff, W. & Bonse, U. (1977). *Z. Phys. B*, **27**, 19–32.
Hart, M. (1968). *J. Phys. D*, **1**, 1405–1408.
Ishikawa, T., Tamasaku, K., Yabashi, M., Goto, S., Tanaka, Y., Yamazaki, H., Takeshita, K., Kimura, H., Ohashi, H., Matsushita, T. & Ohata, T. (2001). *Proc. SPIE*, **4145**, 1–10.
Kincaid, B. M. (1977). *J. Appl. Phys.* **48**, 2684–2691.
Madey, J. M. J. (1971). *J. Appl. Phys.* **42**, 1906–1913.
Mandel, L. (1961). *J. Opt. Soc. Am.* **51**, 1342–1350.
Murphy, J. B. & Pellegrini, C. (1985). *Nucl. Instrum. Methods Phys. Res. A*, **237**, 159–167.
Nishino, Y. & Tamasaku, K. (2001). *BL29XU RIKEN Coherent X-ray Optics*, http://www.spring8.or.jp/e/facility-e.html.
Nusshardt, M. & Bonse, U. (2003). *J. Appl. Cryst.* **36**, 269–279.
Pellegrini, C. (1992). *Proceedings of the Workshop on Fourth Generation Light Sources*, pp. 364–375. Stanford: SLAC.
Saldin, E. L., Schneidmiller, E. A., Shvyd'ko, Yu. V. & Yurkov, M. V. (2001). *TESLA Technical Design Report*, Part V (CD-Rom), *XFEL with a meV Bandwidth. Seeding Option.* Hamburg: DESY.
Sutter, J. P., Kuetgens, U., Materlik, G. & Rostomyan, A. (2003). *J. Appl. Cryst.* **36**, 1432–1439.
Tamasaku, K., Tanaka, Y., Yabashi, M., Yamazaki, H., Kawamura, N., Suzuki, M. & Ishikawa, T. (2001). *Nucl. Instrum. Methods Phys. Res. A*, **467/468**, 686–689.
Tanaka, T. (2001). *SPring-8 Inf.* **6**, 113–115.
TESLA (1995). *A VUV Free Electron Laser at the TESLA Test Facility at DESY (Conceptual Design Report)*, ch. 9. Hamburg: DESY.
TESLA (2001). *TESLA Technical Design Report.* ISBN 3-935702-00-0. Hamburg: DESY.
Würges, J., Rostomyan, A. M., Graeff, W. & Materlik, G. (1999). *J. Appl. Cryst.* **32**, 1152–1156.